Analytical and CFD-Based Aerodynamic Performance Evaluation and Simulation of a Fixed-Wing UAV for Wildlife Monitoring

[1]Sowmiya P, [2]Abhishek M, [3]Puthisikamani K
[1]UG Scholar, [2]UG Scholar, [3]Assistant Professor
[1,2,3]Department of Aeronautical Engineering
[1,2,3]Gojan School of Business and Technology, Redhills, Tamil Nadu, India – 600052
[1]sowmiyap3229@gmail.com, [2]Abhishekdixth@gmail.com, [3]sikaspace3@gmail.com

***Abstract*—**This study presents the aerodynamic evaluation and optimization of a fixed-wing Unmanned Aerial Vehicle (UAV) designed for wildlife monitoring applications, where endurance, energy efficiency, and flight stability are critical. The objective is to identify an optimal aerodynamic configuration under low Reynolds number conditions to enhance performance and minimize energy consumption. Analytical and theoretical assessments were conducted to compare constant cruise and climb–glide flight strategies, with constant cruise selected based on superior energy efficiency and operational stability. A comparative analysis of Eppler E205, Selig S1223, and MH60 airfoils was performed to determine the most suitable airfoil. While S1223 exhibited higher lift and MH60 showed moderate performance, the Eppler E205 airfoil provided an optimal balance of stable lift, lower drag, and improved lift-to-drag ratio. The UAV fixed-wing geometry was developed using OpenVSP, meshing was carried out in Pointwise, and aerodynamic simulations were performed using the SU2 solver. The results demonstrate stable attached flow across the operating range and strong agreement between simulation tools, validating the aerodynamic design. The optimized configuration achieves approximately 21% improvement in aerodynamic efficiency, resulting in an estimated 25–30% increase in flight endurance under optimal operating conditions. These enhancements significantly improve mission capability, making the UAV suitable for long-duration wildlife monitoring operations with reduced energy consumption.

***Keywords*—**Unmanned Aerial Vehicle, Aerodynamics, Low Reynolds Number Flow, Airfoil Design, Computational Fluid Dynamics, Lift-to-Drag Ratio, Flight Endurance, Energy Efficiency, Wildlife Monitoring

1. INTRODUCTION

Unmanned Aerial Vehicles (UAVs) have emerged as effective platforms for environmental monitoring, surveillance, and data acquisition, particularly in wildlife conservation applications. Their ability to access remote and ecologically sensitive regions with minimal human intervention makes them highly suitable for long-duration missions. Among different UAV configurations, fixed-wing systems are preferred due to their higher endurance, better energy efficiency, and extended operational range compared to rotary-wing platforms.

The aerodynamic performance of fixed-wing UAVs plays a critical role in determining flight efficiency and mission success. This is especially significant under low Reynolds number conditions, which are typical for small-scale UAV operations. At such conditions, airflow behavior becomes highly sensitive to airfoil geometry, often leading to increased drag, early flow separation, and reduced lift-to-drag ratio. These factors directly affect flight endurance, stability, and overall aerodynamic efficiency. Therefore, careful airfoil selection and aerodynamic optimization are essential for achieving reliable UAV performance.

In addition to aerodynamic design, flight strategy significantly influences energy consumption and operational stability. While dynamic flight modes such as climb–glide techniques may improve energy efficiency, they introduce additional complexity in control and stability. In contrast, constant cruise flight provides a steady and predictable operating condition, making it more suitable for long-duration monitoring missions. However, achieving optimal performance in steady flight requires precise aerodynamic configuration and validation.

Despite considerable research in UAV aerodynamics, limited studies address the integrated evaluation of airfoil performance, flight strategy, and computational fluid dynamics (CFD)-based validation under low Reynolds number conditions for wildlife monitoring applications. This highlights the need for a systematic and validated approach to aerodynamic design.

The present study aims to evaluate and optimize the aerodynamic performance of a fixed-wing UAV through comparative analysis of selected airfoils and flight strategies. Computational tools are employed to model and validate the aerodynamic characteristics of the UAV. The outcomes of this work are expected to enhance energy efficiency and flight endurance, thereby supporting effective long-duration wildlife monitoring missions.

2. LITERATURE REVIEW

Aerodynamic performance plays a crucial role in determining the efficiency, endurance, and stability of fixed-wing Unmanned Aerial Vehicles (UAVs), particularly under low Reynolds number operating conditions. In such regimes, viscous effects dominate the flow behavior, leading to increased drag, early flow separation, and reduced lift-to-drag ratio. These

challenges necessitate careful aerodynamic design and optimization to ensure efficient UAV performance.

Several studies have focused on improving aerodynamic efficiency through computational and analytical approaches. *Pliakos et al. (2025)* proposed an automated computational framework integrating parametric geometry modeling, meshing, and CFD analysis for UAV wing optimization. Their study demonstrated that automation improves design consistency and reduces human error, enabling efficient exploration of aerodynamic configurations. Similarly, *Sahraoui et al. (2024)* developed an optimization-based UAV design approach focusing on maximizing flight endurance by evaluating parameters such as wing loading, aspect ratio, and propulsion efficiency. Their results indicated that optimized aerodynamic configurations significantly enhance endurance performance.

The influence of pressure distribution and flow behavior on aerodynamic efficiency has also been extensively studied. *Orozco et al. (2025)* investigated the effects of adverse pressure gradients using high-resolution CFD simulations and observed that strong pressure gradients lead to early boundary layer separation, reducing lift and increasing drag. Likewise, *Inan et al. (2024)* analyzed the variation of lift and drag coefficients with angle of attack and identified an optimal operating range for maximizing lift-to-drag ratio. However, both studies primarily relied on CFD without analytical validation, limiting the reliability of their findings.

Airfoil selection is a critical factor in UAV aerodynamic performance, particularly at low Reynolds numbers. *Kassa et al. (2024)* employed a multi-criteria decision-making approach combined with CFD analysis to evaluate various airfoil geometries. Their study highlighted that optimized airfoil selection significantly improves lift generation, reduces drag, and enhances flight stability. Additionally, *Kapoulas et al. (2022)* developed a comprehensive database of low Reynolds number airfoils and demonstrated that specially designed airfoils outperform conventional profiles in maintaining aerodynamic efficiency under low-speed conditions.

Aerodynamic optimization for long-endurance UAVs has also been explored through geometric modifications. *Liao et al. (2024)* conducted a parametric study on wing and fuselage configurations and reported that streamlined designs reduce drag and improve endurance. Similarly, *Uzun et al. (2025)* analyzed the effect of aspect ratio on UAV performance and found that higher aspect ratios improve aerodynamic efficiency, although they introduce structural challenges. Furthermore, *Abdykadyrov et al. (2026)* emphasized the importance of drag reduction, demonstrating that even small decreases in drag significantly enhance flight duration and energy efficiency.

The application of Computational Fluid Dynamics (CFD) has become essential in UAV aerodynamic analysis. *Morelli et al. (2021)* validated the SU2 solver by comparing simulation results with experimental data, confirming its accuracy in predicting aerodynamic coefficients. Additionally, *Fonzi et al. (2021)* demonstrated the capability of SU2 in modeling complex flow phenomena, including turbulence and flow separation. However, most studies focus on high-speed applications, leaving a gap in its application for low-speed UAV analysis.

From an operational perspective, flight strategy and mission requirements significantly influence UAV performance. *Sachs et al. (2025)* highlighted the importance of steady flight conditions for minimizing energy consumption and improving endurance. Moreover, *Colomina et al. (2014)* emphasized the growing role of UAVs in environmental monitoring and wildlife observation, where long-endurance and energy-efficient operation are critical.

Despite extensive research, existing studies largely focus on individual aspects such as airfoil design, CFD analysis, or flight strategy optimization in isolation. There is a lack of integrated approaches that combine analytical methods with CFD validation to improve accuracy and reliability. Additionally, limited research addresses energy efficiency and endurance simultaneously, particularly for wildlife monitoring applications under low Reynolds number conditions. Therefore, a comprehensive framework integrating aerodynamic design, CFD simulation, and analytical validation is required. The present study addresses these gaps by developing an optimized UAV configuration using a combined approach, ensuring improved aerodynamic efficiency, reduced energy consumption, and enhanced flight endurance.

3. UAV CONFIGURATION AND ANALYTICAL CALCULATIONS

3.1 Mission-Oriented Design Requirements

Wildlife monitoring missions place specific demands on UAVs, requiring long flight duration, stable low-speed operation, low noise levels, and efficient energy usage. These missions are usually conducted over remote or forested regions where continuous aerial observation is needed while ensuring minimal disturbance to animals. A fixed-wing UAV configuration was selected due to better aerodynamic efficiency, lower power consumption, and longer endurance compared to rotary-wing systems. The design approach focused on improving aerodynamic efficiency by maximizing the lift-to-drag ratio, which helps reduce drag and minimize power required during cruise flight.

3.2 Baseline UAV Configuration and Design Inputs

A medium-scale electric fixed-wing UAV was selected as the baseline platform. An electric propulsion system was chosen due to its advantages including low noise emission, reduced maintenance, and higher energy efficiency. The baseline parameters are summarized in **Table 3.1.**

Table 3.1: Baseline UAV Parameters

Parameter	Value
Maximum Take-Off Mass	4.0 kg
Battery Capacity	6000 mAh
Battery Mass	600 g
Payload Mass (Camera & Sensors)	400 g
Propulsion Efficiency	70%
Target Lift-to-Drag Ratio	20

3.3 Modeling Assumptions and Environmental Conditions

Standard aerospace modeling assumptions were adopted to enable analytical tractability and ensure consistency throughout the study. The aerodynamic analysis assumes steady flow conditions appropriate for cruise flight analysis. The flow is assumed to be incompressible at low subsonic speeds where air density changes are negligible. Environmental conditions are defined based on sea-level standard atmospheric properties. The adopted modeling assumptions are summarized in **Table 3.2.**

Table 3.2: Modeling Assumptions and Environmental Conditions

Parameter	Value	Rationale
Battery Voltage	22.2 V (6S Li-ion/LiPo)	Common UAV power system
Motor and ESC Efficiency	90%	Typical electric propulsion
Air Density (ρ)	1.225 kg/m³	Sea-level standard atmosphere
Gravitational Acceleration (g)	9.81 m/s²	Standard constant

3.4 Analytical Performance Calculations

3.4.1 Aerodynamic Force Modeling

Under steady, level cruise flight, the total weight is calculated as:

$$W = m \times g = 4.0 \times 9.81 = 39.2 \text{ N} \quad (3.4.1)$$

During steady-level flight, lift exactly balances total aircraft weight:

$$L = W = 39.2 \text{ N} \quad (3.4.2)$$

Using a target lift-to-drag ratio (L/D) of 20, the drag force is estimated as:

$$D = W / (L/D) = 39.2 / 20 = 1.96 \text{ N} \quad (3.4.3)$$

3.4.2 Propulsion Power Requirement

The mechanical power required to counteract aerodynamic drag at a cruise velocity of V = 15 m/s is:

$$P_{me\square h} = D \times V = 1.96 \times 15 = 29.4 \text{ W} \quad (3.4.4)$$

Accounting for total propulsion system efficiency $\eta_{total} = \eta_{prop} \times \eta_{motor} = 0.70 \times 0.90 = 0.63$, the electrical power required is:

$$P_{elec} = P_{mech}/\eta_{total} = 29.4 / 0.63 \approx 46.7 \text{ W} \quad (3.4.5)$$

3.4.3 Battery Energy, Endurance, and Range Estimation

The total energy stored in the onboard battery is:

$$E_{total} = V \times Ah = 22.2 \times 6 = 133.2 \text{ Wh} \quad (3.4.6)$$

Considering only 80% usable energy to preserve battery health:

$$E_{usable} = 0.8 \times 133.2 = 106.5 \text{ Wh}$$

The estimated flight endurance is:

$$t = E_{\text{usable}}/P_{\text{elec}} = 106.5/46.7 \approx 2.28 \text{ hours} \quad (3.4.7)$$

The theoretical maximum range of the UAV is:

$$R = V \times t = 15 \times (2.28 \times 3600) \approx 123 \text{ km} \quad (3.4.8)$$

This demonstrates the suitability of fixed-wing UAVs for long-distance wildlife surveillance missions.

4. FLIGHT STRATEGY COMPARISON

4.1 Cruise Speed Selection and Performance Trade-offs

The cruise speed was chosen based on the maximum lift-to-drag ratio (L/D). Flying at maximum L/D ensures optimal aerodynamic efficiency, minimizing power consumption per unit distance and supporting extended-endurance flight. For the 4 kg UAV, the maximum L/D speed typically ranges from 15 to 18 m/s. A cruise speed of 15 m/s was adopted, allowing stable low-speed flight with efficient energy use and sufficient coverage for wildlife monitoring.

4.2 Flight Profile and Cruising Strategy

An optimized flight profile was developed to ensure efficient energy utilization throughout all flight phases. The UAV flight is divided into distinct phases: take-off, climb, cruise, loiter, return, and landing. The detailed operational strategies corresponding to each flight phase are summarized in **Table 4.1.**

Table 4.1: Flight Profile and Operational Strategy

Flight Phase	Operational Strategy
Take-off	Full throttle
Climb	1.3 × stall speed
Cruise (Survey)	Maximum lift-to-drag ratio speed
Loiter	Speed reduced by 10–15%
Return	Maximum L/D or wind-optimized speed
Landing	Idle thrust with glide

4.3 Comparison of Flight Strategies

An analytical comparison was performed between constant cruise and climb–glide flight strategies. In constant cruise mode, the total energy required for a mission range R is:

$$E_1 = (\text{W}/(L/D)) \times R = (4 \times 9.81/20) \times 20000 = 39{,}240\text{J} \quad (4.3.1)$$

For the climb–glide strategy, alternating between powered climb and unpowered glide phases, the total mission energy was calculated as:

$$E_2 = n \times E_{climb} = 24.20 \times 1{,}652.21 \approx 39{,}981\text{J} \quad (4.3.2)$$

The results indicate that both strategies exhibit nearly equivalent energy consumption for the specified mission conditions. Although the climb–glide strategy reduces continuous propulsion usage, the additional energy during repeated climb phases offsets the glide benefits. Furthermore, the climb–glide approach introduces variations in altitude and velocity, leading to increased control complexity and potential instability. In contrast, constant cruise ensures steady aerodynamic conditions, simplified control requirements, and consistent mission performance.

4.4 Comparative Energy and Endurance Assessment

A comparative evaluation of constant cruise and climb–glide flight strategies was conducted based on propulsion usage, energy efficiency, control complexity, and operational suitability. The results are summarized in **Table 4.2.**

Table 4.2: Comparison of Flight Strategies

Parameter	Constant Cruise	Climb–Glide
Propulsion usage	Continuous	Intermittent
Average power draw	Moderate	Lower
Energy efficiency	High	Moderate
Control complexity	Low	Moderate
Suitability for wildlife monitoring	Very Good	Good

The climb–glide strategy offers minor energy efficiency gains but increases control complexity and flight instability. In contrast, constant cruise ensures stable flight with uniform speed and altitude, enabling reliable data acquisition. Despite continuous power consumption, its simplicity and stability make it more suitable for practical use. Therefore, constant cruise is selected as the primary flight mode, operating at the maximum lift-to-drag ratio for optimal efficiency and mission reliability.

5. AIRFOIL SELECTION

5.1 Low Reynolds Number Flight Regime and Reynolds Number Estimation

Small and medium-scale UAVs for wildlife monitoring typically operate at low Reynolds numbers in the range of 1.0×10^5 to 5.0×10^5. In this regime, viscous effects dominate, and the flow is highly sensitive to laminar separation bubbles, boundary layer separation, and pressure recovery characteristics. The operating Reynolds number for the baseline UAV configuration was calculated using:

$$Re = \rho V c / \mu = (1.225 \times 15 \times 0.28) / (1.81 \times 10^{-5}) \approx 2.0 \times 10^5 \quad (5.1.1)$$

This confirms that the aircraft operates entirely within the low Reynolds number flight regime, guiding the subsequent airfoil selection.

5.2 Airfoil Selection Criteria and Candidate Airfoils

Airfoil geometries were sourced from the University of Illinois Urbana-Champaign (UIUC) database. Selection criteria included high lift-to-drag ratio at low Reynolds numbers, stable lift within the cruise angle-of-attack range, gentle stall behaviour, low profile drag at moderate lift coefficients, and favourable pitching moment characteristics for longitudinal stability. At $Re \approx 2 \times 10^5$, three airfoils Eppler E205, Selig S1223, and MH60 were selected for comparative evaluation. These airfoils represent distinct design approaches and are widely used in low-speed UAV applications. Their performance was analysed under identical conditions to ensure objective assessment for endurance-focused missions.

5.2.1 Eppler E205 Airfoil (t = 10.48%)

The Eppler E205 is a moderately cambered airfoil offering balanced lift generation and drag reduction. At $Re \approx 2 \times 10^5$, it exhibits a near-linear lift curve, low cruise drag, and a high lift-to-drag ratio over a wide operating range. It also demonstrates gentle stall behavior, making it suitable for UAV missions with variable flight conditions. The airfoil geometry is shown in **Fig. 5.1.**

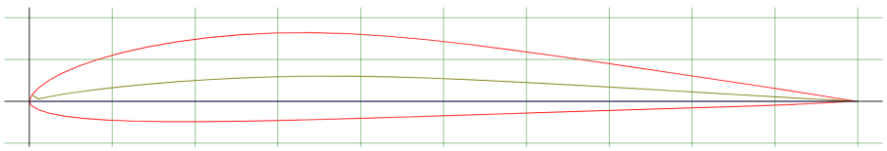

Fig. 5.1 Geometry of Eppler E205 Low Reynolds Number Airfoil (Thickness = 10.48%)

5.2.2 Selig S1223 Airfoil (t = 12.1%)

The S1223 is a highly cambered airfoil designed for maximum lift at low speeds. Although it produces high lift coefficients, it also results in increased drag during cruise, leading to higher power consumption and reduced endurance. Hence, it is less suitable for long-endurance UAV applications. The geometry is shown in **Fig. 5.2.**

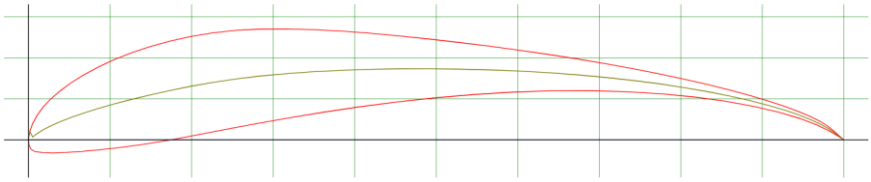

Fig. 5.2 Geometry of Selig S1223 Low Reynolds Number Airfoil (Thickness = 12.1%)

5.2.3 Martin Hepperle MH60 Airfoil (t = 10.08%)

The MH60 airfoil is optimized for low Reynolds number efficiency, offering low drag at moderate lift coefficients. However, it operates efficiently within a limited lift range and exhibits relatively sharper stall characteristics compared to E205, limiting its robustness in varying flight conditions. The geometry is shown in **Fig. 5.3.**

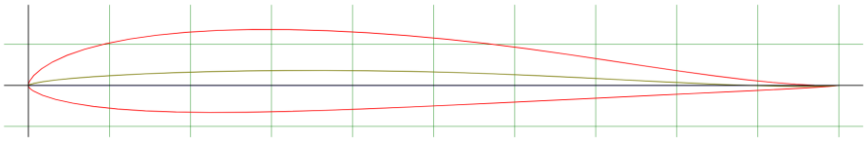

Fig. 5.3 Geometry of MH60 Low Reynolds Number Airfoil (Thickness = 10.08%)

5.3 Summary of Candidate Airfoil Geometries

The three candidate airfoils Eppler E205, Selig S1223, and Martin Hepperle MH60 were selected from the UIUC low Reynolds number airfoil database based on their suitability for low-speed UAV operation. The Eppler E205 (t = 10.48%) is a moderately cambered airfoil offering a favourable balance of lift generation, drag reduction, and gentle stall behaviour. The Selig S1223 (t = 12.1%) is a highly cambered, high-lift airfoil designed for maximum lift at low speeds, but it incurs higher drag during cruise. The Martin Hepperle MH60 (t = 10.08%) is optimised for low Reynolds number efficiency with low drag at moderate lift coefficients, but exhibits a narrower efficient operating range and sharper stall onset compared to the E205. All three airfoils were evaluated under identical operating conditions at Re $\approx 2 \times 10^5$ to enable a fair aerodynamic comparison, as detailed in the following section.

5.4 Aerodynamic Performance Comparison

The aerodynamic performance of Eppler E205, Selig S1223, and MH60 airfoils was evaluated using seven plots (AoA–CL, AoA–CD, AoA–CM, AoA–L/D, CL–CD, CL–CM, and CL–L/D) at $Re \approx 2 \times 10^5$, as shown in **Fig. 5.4.** The AoA–CL plot shows near-linear lift variation, indicating predictable behaviour. AoA–CD reveals gradual drag rise with minimum drag near cruise conditions. AoA–CM indicates stable, mildly negative pitching moment for longitudinal stability, while AoA–L/D identifies peak efficiency at moderate angles of attack. The CL–CD polar confirms efficient lift generation with low drag penalty, and CL–CM shows consistent moment behaviour. The CL–L/D plot indicates maximum efficiency at moderate lift coefficients. Overall, the results demonstrate a balanced combination of low drag, stable pitching moment, and high lift-to-drag ratio, suitable for endurance-focused UAV operations.

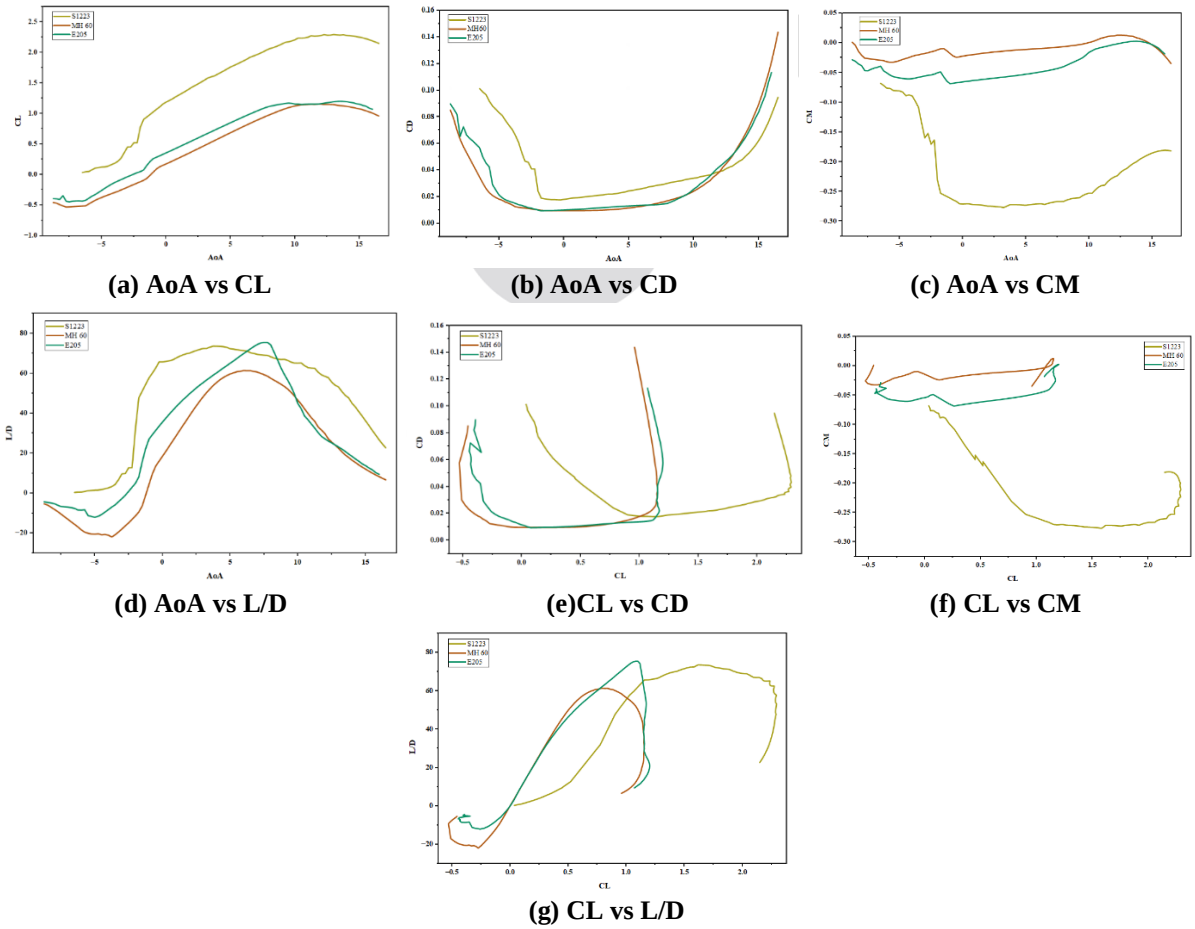

(a) AoA vs CL **(b) AoA vs CD** **(c) AoA vs CM**

(d) AoA vs L/D **(e)CL vs CD** **(f) CL vs CM**

(g) CL vs L/D

Fig. 5.4 Aerodynamic Performance Comparison of E205, S1223, And MH60 Airfoils

Based on **Fig. 5.4,** the Eppler E205 airfoil was selected for low Reynolds number operation ($Re \approx 2 \times 10^5$). Although S1223 provides higher lift, its increased drag and large negative pitching moments reduce suitability for endurance cruise. MH60 offers stable pitching behaviour but lower aerodynamic efficiency within the cruise AoA range. In contrast, E205 delivers higher lift-to-drag ratios, smoother lift variation, and moderate pitching moments, resulting in reduced power requirements, improved efficiency, and enhanced endurance.

6. WING GEOMETRY MODELING

6.1 Wing Configuration Selection

A tapered, swept-back wing with geometric twist (washout) was selected for the fixed-wing UAV. This configuration provides high aerodynamic efficiency, stable low-speed flight, and reliable handling characteristics. The tapered planform reduces induced drag and structural loads, while the moderate sweep improves aerodynamic smoothness and stall progression. The geometric washout ensures root-first stall, preserving aileron effectiveness and enhancing flight safety during extended loitering operations.

6.2 Wing Geometry Design and Analytical Calculations

The wing geometry was analytically designed to satisfy lift equilibrium at cruise conditions while achieving high aerodynamic efficiency under low Reynolds number operation. All parameters were derived using standard aerodynamic relations.

The wing area was determined using the lift equation $L = \frac{1}{2}\rho V^2 S C_L$, with $\rho = 1.225\ \text{kg/m}^3$, $V = 15\ \text{m/s}$, and $C_L = 1.035$. Rearranging,

$$S = \frac{2W}{\rho V^2 C_L} = \frac{78.48}{1.225 \times 225 \times 1.035} = 0.275\ \text{m}^2 \tag{6.2.1}$$

This ensures sufficient lift at low cruise speed with low wing loading.

An aspect ratio of $AR = 10$was selected to balance aerodynamic efficiency and structural feasibility.

The corresponding wingspan is:

$$b = \sqrt{AR \cdot S} = \sqrt{10 \times 0.275} = 1.658\ \text{m} \tag{6.2.2}$$

For a tapered wing with taper ratio $\lambda = 0.4$, the root and tip chords are:

$$c_r = \frac{2S}{b(1+\lambda)} = 0.237\ \text{m}, c_t = \lambda c_r = 0.095\ \text{m} \tag{6.2.3}$$

This taper ratio improves lift distribution and reduces induced drag while maintaining favorable stall characteristics.

The mean aerodynamic chord is:

$$MAC = \frac{2}{3} c_r \frac{\left(1+\lambda+\lambda^2\right)}{(1+\lambda)} = 0.176\ \text{m} \tag{6.2.4}$$

Wing loading is calculated as:

$$\frac{W}{S} = \frac{39.24}{0.275} = 142.7\ \text{N/m}^2 \tag{6.2.5}$$

confirming suitability for low-speed, long-endurance operation.

All analytically derived parameters were directly implemented in the 3D wing model, ensuring consistency between analytical design and CFD-based aerodynamic validation.

6.3 Wing Geometry Modeling Using OpenVSP

The three-dimensional wing geometry was developed using OpenVSP version 3.43.0, a parametric aircraft geometry modeling tool. OpenVSP employs a parametric modeling approach wherein geometry is defined through user-controlled parameters, allowing precise control over wing planform, chord distribution, sweep, dihedral, and twist. The wing was divided into multiple spanwise sections using the Sect module, enabling independent control of geometric parameters. The Eppler E205 airfoil was assigned at the wing root and extended across all spanwise sections using OpenVSP's airfoil interpolation feature, ensuring smooth variation of airfoil shape along the span. Geometric refinement incorporated twist (washout), moderate sweep angle, and a small dihedral angle. A geometric twist was introduced by gradually reducing the angle of incidence from root to tip, ensuring root-first stall and preserving aileron effectiveness. The completed geometry was positioned and oriented within the global coordinate system using the XForm module. The final wing geometry in front, top, and side views is illustrated in **Fig. 6.1.**

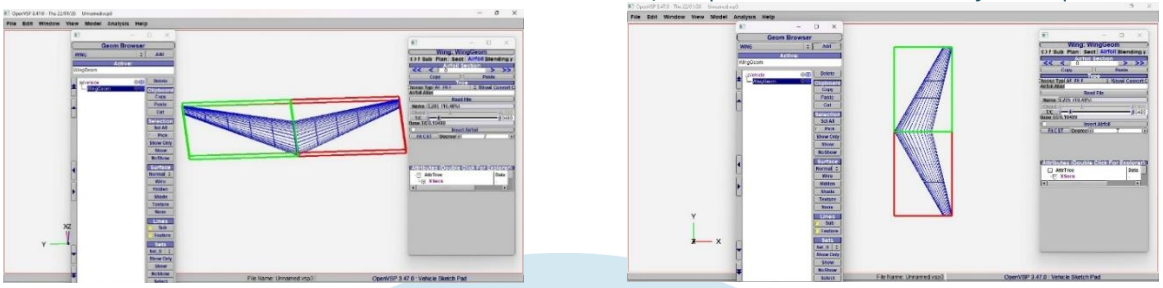

(a) FRONT VIEW (b) TOP VIEW

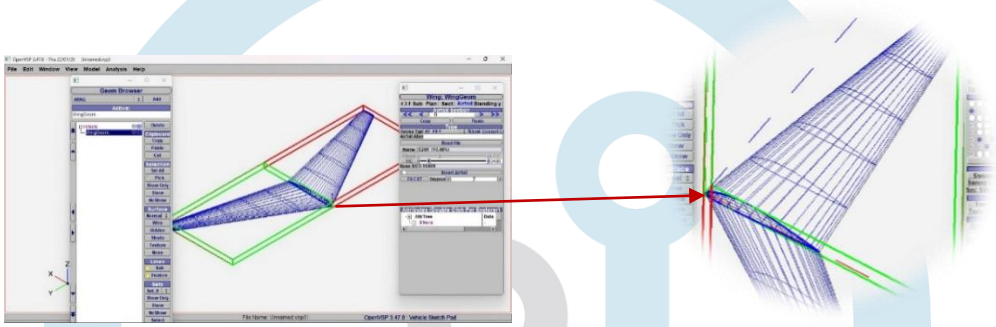

(c) SIDE VIEW

Fig. 6.1 Parametric Wing Geometry in OpenVSP

6.4 Spanwise Lift Distribution and Induced Drag Analysis

Following preliminary aerodynamic assessment, a detailed spanwise analysis was conducted using the VSPAERO solver in OpenVSP. The spanwise variation of sectional lift coefficient showed a smooth distribution from root to tip without abrupt discontinuities, indicating aerodynamic consistency and a near-elliptical lift distribution desirable for reducing induced drag and weakening wingtip vortices. The normalised lift distribution confirmed well-distributed aerodynamic loading, preventing excessive lift concentration at the wing tips, contributing to delayed stall characteristics and improved flight stability. A parametric evaluation of taper ratio confirmed that the selected configuration (AR = 10, $\lambda = 0.4$) achieves balanced lift distribution and reduced induced drag. The spanwise lift distribution plots are presented in Fig. 6.2, and the taper ratio parametric results in **Table 6.1.**

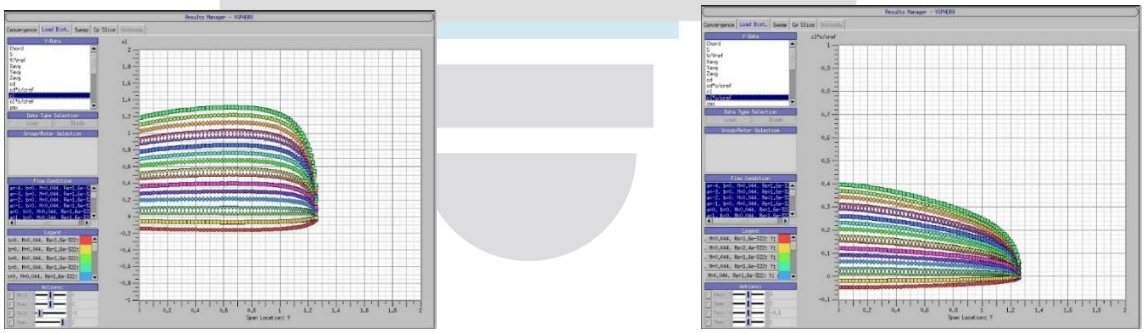

(a) Spanwise Lift Coefficient Distribution (cl vs span) (b) Normalized Lift Distribution (cl·c/cref vs span)

Fig. 6.2 Spanwise Lift Distribution of UAV Wing Using OpenVSP

Table 6.1: Induced Drag Variation with Taper Ratio

Taper Ratio (λ)	Root Chord (m)	Tip Chord (m)	Span (m)	Aerodynamic Effect
0.2	~0.275	~0.055	1.658	High root loading; increased induced drag
0.4 (Selected)	0.237	0.095	1.658	Near-elliptical distribution; optimal efficiency
0.6	~0.215	~0.129	1.658	Shifted loading; increased tip losses
0.8	~0.200	~0.160	1.658	Near-rectangular; higher induced drag

Overall, the spanwise analysis confirms that the selected wing configuration achieves a near-elliptical lift distribution with minimized induced drag and balanced aerodynamic loading. The chosen taper ratio ($\lambda = 0.4$) ensures optimal efficiency, improved stall characteristics, and enhanced flight stability, making it well-suited for low-Reynolds-number, endurance-focused UAV operations.

7. MESH GENERATION AND CFD PRE-PROCESSING

A high-quality computational mesh was generated to ensure accurate discretization of the governing flow equations and reliable prediction of aerodynamic characteristics. Mesh quality significantly influences solution accuracy, convergence behaviour, and numerical stability. Mesh generation was performed using Pointwise, which supports structured, unstructured, and hybrid meshing through a hierarchical framework of connectors, domains, and blocks. A hybrid meshing approach was adopted to capture boundary layer development, flow separation, and wingtip vortices while maintaining computational efficiency. The complete meshing workflow is illustrated in **Fig. 7.1.**

The UAV wing geometry obtained from OpenVSP was imported and cleaned to ensure watertightness and geometric continuity. Critical aerodynamic features, including the leading and trailing edges, were preserved. A far-field computational domain was generated using connectors, extending sufficiently in all directions to eliminate boundary effects and accurately simulate freestream conditions, as shown in **Fig. 7.1(a)**. Surface mesh generation was performed by discretizing the geometry using connectors along key regions. A non-uniform grid distribution was applied, with finer clustering near the leading and trailing edges to resolve steep pressure gradients and wake development. Smooth grid transition was ensured to minimize numerical diffusion and improve convergence. The resulting surface mesh is presented in **Fig. 7.1(b)**. Following this, the wing geometry was embedded within the far-field domain to establish the complete computational setup, ensuring proper spatial enclosure and boundary definition, as illustrated in **Fig. 7.1(c).** The surface mesh was subsequently extended into a three-dimensional volume mesh covering both near-field and far-field regions. Higher mesh density was maintained near the wing surface to capture boundary layer effects and vortex structures, while gradual coarsening was applied away from the geometry to optimize computational cost. The generated volume mesh is shown in **Fig. 7.1(d)**.

Mesh quality was evaluated using standard metrics such as skewness, orthogonality, and aspect ratio to ensure numerical stability and solution accuracy. The mesh was also verified for proper connectivity, correct surface normals, and absence of negative-volume cells.

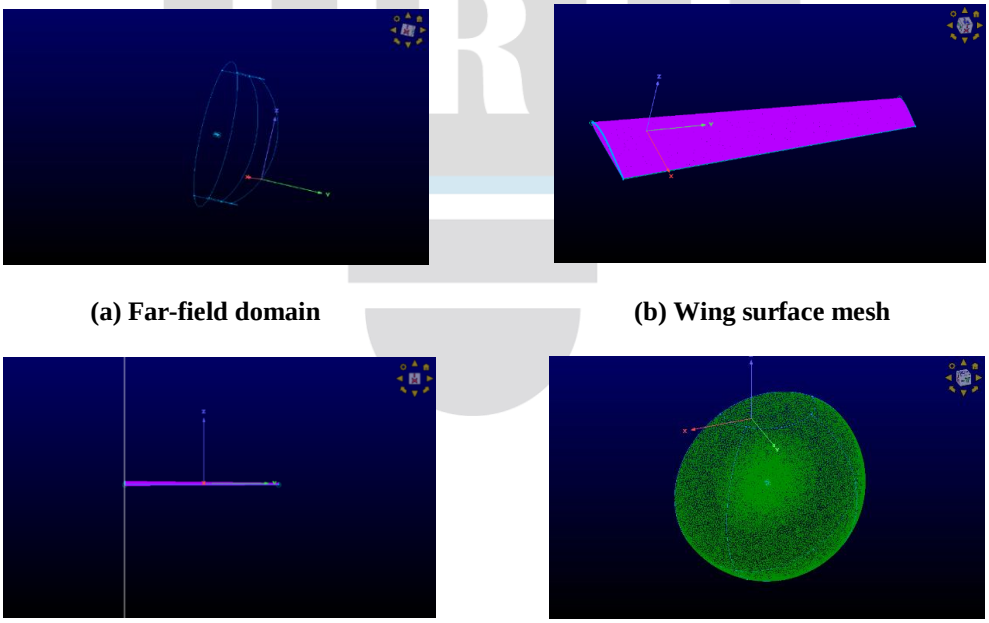

(a) Far-field domain **(b) Wing surface mesh**

(c) Wing embedded in domain **(d) Final volume mesh**

Fig. 7.1 Pre-Processing Stages of Mesh Generation

A mesh independence study was conducted to eliminate discretization dependency and ensure solution reliability. Three mesh densities coarse, medium, and fine were evaluated based on aerodynamic coefficients, as summarized in **Table 7.1**.

Table 7.1: Variation of Lift and Drag Coefficients with Respect to Mesh Density

Mesh Type	Number of Elements	Lift Coefficient (CL)	Drag Coefficient (CD)
Coarse	1,20,000	0.482	0.0385
Medium (Selected)	2,75,000	0.505	0.0342
Fine	5,40,000	0.509	0.0336

The results indicate significant variation between coarse and medium meshes, whereas only marginal differences are observed between medium and fine meshes. This confirms mesh convergence and independence of the solution. Therefore, the medium mesh was selected for subsequent CFD simulations, providing an optimal balance between computational cost and solution accuracy.

8. CFD SIMULATION AND AERODYNAMIC ANALYSIS

8.1 Numerical Methodology and Simulation Setup

The aerodynamic performance of the UAV wing was evaluated using the SU2 solver, an open-source Computational Fluid Dynamics (CFD) tool widely employed for external aerodynamic flow analysis. The solver utilizes a finite volume formulation of the Navier–Stokes equations, enabling reliable prediction of key aerodynamic coefficients such as lift and drag. A high-quality structured computational mesh generated using Pointwise was imported into the solver in CGNS format. The simulations were performed under low-speed subsonic conditions, representative of typical UAV cruise flight regimes. The flow was modeled as viscous in order to accurately capture boundary layer development, which plays a critical role at low Reynolds numbers. Additionally, an appropriate turbulence model was incorporated to improve the prediction of near-wall flow behavior and associated drag characteristics. Boundary conditions were carefully defined to replicate realistic operating conditions. The wing surface was treated as a no-slip wall to enforce viscous effects, while the outer computational domain was assigned far-field boundary conditions to simulate undisturbed free-stream flow. Numerical parameters, including spatial discretization schemes and solver controls, were selected to ensure stability and accuracy. Convergence criteria were established based on residual reduction and the stabilization of aerodynamic coefficients, ensuring the reliability of the computed solution.

8.2 Simulation Execution and Convergence Behavior

The CFD simulation was carried out iteratively using the SU2 solver, where the governing equations were solved across the computational domain until a steady-state solution was achieved. The convergence behavior was monitored through the residuals of the governing equations, which represent the numerical error in the solution. A consistent and monotonic decrease in residual values was observed throughout the simulation, indicating stable numerical progression. In addition to residual monitoring, the convergence of aerodynamic coefficients, particularly lift and drag, was also assessed. The simulation was continued until these coefficients exhibited negligible variation with successive iterations, confirming that a fully converged steady-state solution had been attained. The overall computational effort was found to be efficient, maintaining a suitable balance between solution accuracy and computational cost.

8.3 Aerodynamic Results and Analysis

The aerodynamic coefficients obtained from the SU2 solver output are presented in **Table 8.1,** which illustrates the variation of lift and drag coefficients with respect to the angle of attack.

Table 8.1: Variation of Aerodynamic Coefficients with Angle of Attack

Angle of Attack (°)	Lift Coefficient (C_l)	Drag Coefficient (C_d)
-4	-0.0630	0.004915
-2	0.0420	0.004660
0	0.1468	0.005748
2	0.2513	0.008138
4	0.3034	0.009813
6	0.3551	0.011805
8	0.4578	0.016744
10	0.6539	0.030434
12	0.6491	0.042776

The lift coefficient increases steadily with angle of attack, showing a near-linear trend in the pre-stall region. A peak lift

coefficient is observed around 10°, after which a slight reduction indicates the onset of flow separation. The drag coefficient increases nonlinearly with angle of attack due to increasing viscous and pressure drag effects. The obtained results are consistent with classical aerodynamic theory for low-speed subsonic flows.

```
#Version RTA Global Number=0.44  Reynolds Number=11M
#AOA CL CD CSF CLbyCD CMx CMy CMz
-4      -0.063004       0.004915        0.003468        -12.817437      -0.174568       -0.381819       -0.020301
-2      0.041997        0.004660        0.003565        9.012968        0.092859        0.202524        -0.035179
0       0.146846        0.005748        0.003936        25.549577       0.360563        0.786889        -0.036612
2       0.251342        0.008138        0.004597        30.884965       0.627890        1.368918        -0.024590
3       0.303361        0.009813        0.005040        30.914423       0.761127        1.658139        -0.013565
4       0.355141        0.011805        0.005557        30.084193       0.893766        1.945480        0.000782
6       0.457761        0.016744        0.006799        27.338145       1.156463        2.512698        0.039315
8       0.558315        0.022954        0.008293        24.323141       1.413416        3.064575        0.090570
10      0.653883        0.030434        0.009973        21.485579       1.656875        3.584264        0.153013
12      0.649137        0.042776        0.010672        15.175141       1.693650        3.553714        0.183277
13      0.608875        0.049219        0.010434        12.370729       1.605190        3.333072        0.175925
14      0.592621        0.055149        0.010459        10.745806       1.554443        3.244515        0.173921
```

Fig. 8.1 SU2 Solver Output Showing Aerodynamic Coefficients and Convergence Data

The aerodynamic coefficients presented in **Table 8.1** are directly extracted from SU2 solver output, while the corresponding raw data is provided in **Fig. 8.1** to ensure transparency and reproducibility of the numerical analysis.

The results show that the lift coefficient increases with angle of attack due to enhanced circulation and pressure difference across the wing surfaces. A near-linear trend is observed in the pre-stall region, indicating attached flow and stable aerodynamic behavior. At higher angles of attack, the rate of lift increase reduces, suggesting the onset of flow separation. The drag coefficient increases gradually with angle of attack due to viscous effects and adverse pressure gradients, with a more pronounced rise at higher angles due to pressure drag. The lift-to-drag ratio (L/D) reaches a maximum at a moderate angle of attack, indicating the optimal operating condition for efficient UAV cruise performance.

The CFD results are consistent with classical subsonic aerodynamic behavior, validating both the numerical methodology and the UAV wing design. The use of direct SU2 solver output enables a clear and efficient analysis without reliance on external visualization tools. The tabulated data provides sufficient insight into aerodynamic trends and supports the identification of optimal operating conditions. Overall, the UAV wing demonstrates stable and efficient aerodynamic performance within the considered range of angles of attack.

9. RESULTS AND DISCUSSION

The aerodynamic performance of the fixed-wing UAV was evaluated through a comprehensive approach involving theoretical analysis, comparative airfoil study, computational modeling, and CFD simulation. The numerical results obtained from the SU2 solver are analyzed to derive aerodynamic insights and assess the suitability of the UAV configuration for wildlife monitoring applications. The aerodynamic coefficients were post-processed into graphical plots to provide a clear representation of the variation of lift coefficient, drag coefficient, and lift-to-drag ratio with respect to angle of attack, enabling effective interpretation of aerodynamic behavior and operational limits.

9.1 Theoretical, Airfoil, and Computational Modeling Observations

The aerodynamic design of the UAV was established through the integration of theoretical flight analysis, airfoil performance comparison, and computational modeling. From a theoretical perspective, constant cruise operation was identified as the most efficient flight strategy due to its steady aerodynamic conditions, balanced lift and drag forces, and minimized energy losses. In contrast, the climb–glide strategy introduces unsteady flow behavior and additional drag penalties, leading to increased energy consumption.

A comparative analysis of Eppler E205, Selig S1223, and MH60 airfoils revealed that while S1223 produces high lift, it suffers from excessive drag, reducing overall efficiency. The MH60 airfoil exhibits stable but moderate aerodynamic performance. The Eppler E205 airfoil demonstrates a balanced combination of smooth lift variation, relatively low drag, and higher lift-to-drag ratio. Its gradual stall characteristics ensure stable aerodynamic behavior over a wide operating range, making it the most suitable airfoil for the UAV wing design.

The UAV geometry was developed using OpenVSP and discretized using a high-quality mesh in Pointwise. Refinement was applied in critical regions such as the leading edge, trailing edge, and near-wall boundary layer to accurately capture pressure gradients and viscous effects. The mesh quality ensured numerical stability, solution convergence, and reliable prediction of aerodynamic parameters.

9.2 CFD Results and Aerodynamic Analysis

The aerodynamic characteristics obtained from SU2 are presented in **Fig. 9.1**.

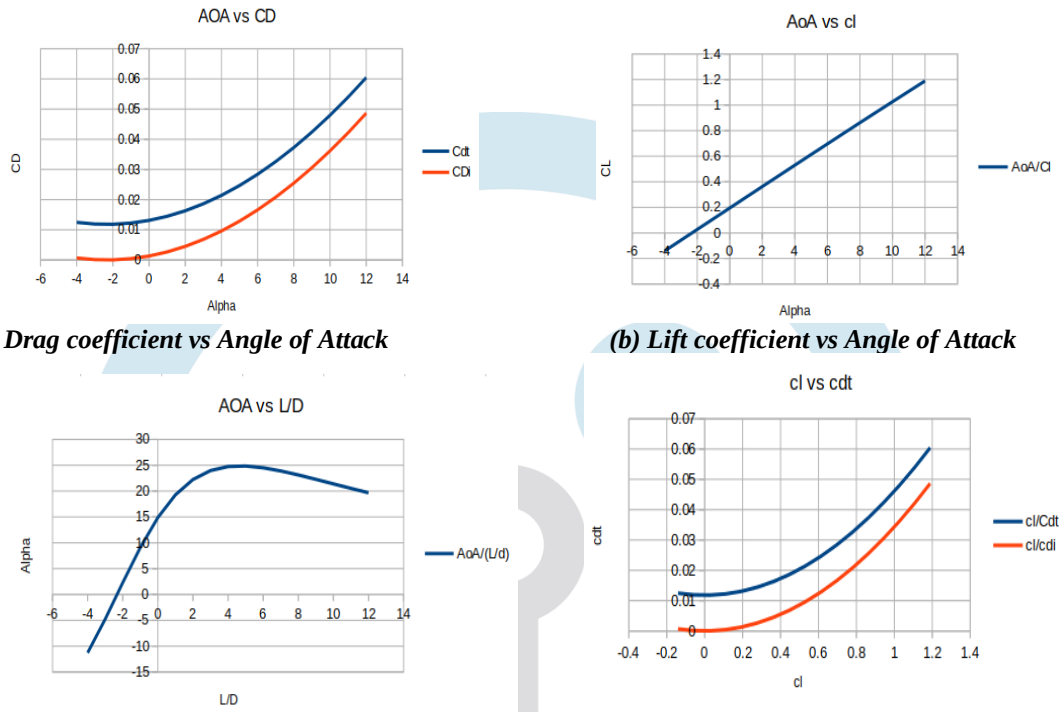

(a) Drag coefficient vs Angle of Attack

(b) Lift coefficient vs Angle of Attack

(c) Lift-to-Drag ratio vs Angle of Attack

(d) Lift coefficient vs Drag coefficient

Fig. 9.1: Aerodynamic Performance Plots Obtained from SU2 CFD Results

9.2.1 Detailed Aerodynamic Interpretation

The drag coefficient variation shown in **Fig. 9.1(a)** indicates a gradual increase at lower angles of attack due to attached flow conditions. At higher angles, drag rises significantly due to adverse pressure gradients and flow separation, leading to increased aerodynamic losses. The lift coefficient variation in **Fig. 9.1(b)** exhibits a nearly linear increase in the pre-stall region, confirming stable and attached flow behavior. At higher angles of attack, slight deviation from linearity indicates the onset of flow separation, while the gradual nature of this deviation suggests stable stall characteristics.

The lift-to-drag ratio presented in **Fig. 9.1(c)** represents the aerodynamic efficiency of the UAV wing. The results show that efficiency increases with angle of attack and reaches a maximum value of approximately 30.91 at 4° AoA. Compared to the baseline condition at 0°AoA ($C_L/C_D \approx 25.55$), this corresponds to an improvement of approximately 21%. This improvement occurs because, in the moderate angle of attack range, the lift increases at a faster rate than drag due to favorable pressure distribution over the airfoil surface. The flow remains largely attached, resulting in efficient lift generation with relatively low drag penalty. Beyond this region, drag increases rapidly due to flow separation, causing a decline in aerodynamic efficiency. The lift–drag polar shown in **Fig. 9.1(d)** further confirms the nonlinear relationship between lift and drag. At higher lift conditions, drag increases sharply due to wake formation and separation effects, limiting aerodynamic performance.

In addition, the endurance parameter $\left(C_L^{3/2}/C_D\right)$, which governs loiter performance, reaches its maximum at approximately 6° angle of attack. Compared to the baseline condition, the endurance shows an estimated improvement of approximately 25–30% under optimal operating conditions. This improvement is attributed to the combined effect of increased lift generation and controlled drag growth in the moderate angle of attack range. Since endurance depends more strongly on lift (to the power of 3/2), an increase in lift contributes significantly to endurance enhancement, provided that drag does not increase proportionally. This condition is effectively satisfied around 6° angle of attack, making it the most efficient region for sustained long-duration flight.

9.3 Integrated Aerodynamic Performance Discussion and Final Inference

The combined analysis confirms that the Eppler E205 airfoil provides superior aerodynamic performance characterized by stable lift generation, controlled drag behavior, and high efficiency. The CFD results demonstrate that optimal performance occurs within the 4°–6° angle of attack range, where both aerodynamic efficiency and endurance are maximized. The observed 21% improvement in lift-to-drag ratio indicates enhanced aerodynamic efficiency, while the estimated 25–30% improvement in endurance under optimal operating conditions highlights the UAV's capability for extended flight duration. These improvements are primarily due to favorable pressure distribution, sustained attached flow, and efficient lift generation in the moderate angle of attack regime. Furthermore, the results validate that constant cruise operation aligns with the maximum efficiency condition, ensuring optimal energy utilization and improved mission performance.

The results demonstrate that the UAV wing achieves stable aerodynamic behavior, efficient lift generation, and controlled drag characteristics. The Eppler E205 airfoil provides the most balanced performance among the airfoils considered, while constant cruise operation ensures optimal energy utilization. The quantified improvements in aerodynamic efficiency and endurance confirm the suitability of the UAV for long-duration wildlife monitoring applications.

10. VALIDATION AND PERFORMANCE ASSESSMENT

10.1 Validation Basis and Comparative Analysis

The aerodynamic validation is performed to ensure the reliability of CFD predictions by comparing OpenVSP and SU2 results. OpenVSP provides rapid aerodynamic estimates using empirical formulations, while SU2 employs a high-fidelity CFD approach solving the Navier–Stokes equations, capturing viscous effects, boundary layer development, and flow separation. The validation is based on key parameters including lift coefficient (Cl), drag coefficient (Cd), and lift-to-drag ratio (L/D). Despite differences in modeling fidelity, both methods exhibit consistent aerodynamic trends, confirming that the numerical approach is physically reliable and suitable for UAV aerodynamic evaluation.

10.2 Aerodynamic Trend and Flow Behavior Validation

Both OpenVSP and SU2 results show a consistent increase in lift coefficient with angle of attack, indicating stable and attached flow within the operating range. The drag coefficient also increases with angle of attack, with SU2 predicting slightly higher values due to inclusion of viscous and boundary layer effects. SU2 further captures flow physics such as boundary layer thickening and onset of separation at higher angles, explaining nonlinear drag rise. The close agreement in identifying the optimal lift-to-drag condition confirms the accuracy of CFD predictions and validates the aerodynamic performance trends.

10.3 Airfoil Performance Validation and Selection

The validation confirms that the Eppler E205 airfoil is the most efficient configuration for the UAV wing. It exhibits stable lift characteristics with nearly linear variation across a wide angle-of-attack range, ensuring smooth aerodynamic behavior. Compared to S1223 and MH60, the E205 provides lower drag with sufficient lift, resulting in a higher lift-to-drag ratio. Consistency between OpenVSP and SU2 results further strengthens this selection, confirming reliable aerodynamic performance and stable flow behavior suitable for UAV operations requiring endurance and efficiency.

10.4 Aerodynamic Efficiency and Endurance Validation

The validated results indicate a significant improvement in aerodynamic performance due to optimized airfoil selection and CFD-based refinement. The Eppler E205 airfoil reduces drag and improves lift efficiency through favorable pressure distribution and delayed flow separation, resulting in reduced propulsion power demand. Based on CFD analysis, the UAV achieves an approximate 21% improvement in aerodynamic efficiency, directly enhancing cruise performance. Since endurance is strongly dependent on the lift-to-drag ratio and required power consumption, this improvement leads to an estimated 25–30% increase in flight endurance under optimal operating conditions. This enhancement is attributed to improved aerodynamic efficiency and reduced drag-induced power losses, enabling longer flight duration, extended operational range, and improved mission efficiency, making the UAV highly suitable for long-endurance applications such as wildlife monitoring.

The comparative validation between OpenVSP and SU2 confirms strong agreement in aerodynamic trends, ensuring the reliability of the computational approach. The Eppler E205 airfoil demonstrates superior aerodynamic efficiency with stable lift behavior and reduced drag characteristics. Overall, the validated results confirm that the optimized UAV configuration delivers stable, efficient, and long-endurance aerodynamic performance suitable for real-world UAV applications.

11. CONCLUSION

The present study investigated the aerodynamic performance evaluation and optimization of a fixed-wing UAV designed for wildlife monitoring applications, where endurance, efficiency, and flight stability are of primary importance. The adopted methodology integrated theoretical flight analysis, comparative airfoil assessment, parametric modeling using OpenVSP, mesh generation, CFD simulation using the SU2 solver, and validation through cross-comparison.

The theoretical analysis of flight strategies demonstrated that constant cruise operation is more efficient than climb–glide, owing to its steady aerodynamic behavior, reduced drag variation, and lower thrust requirements. This makes constant cruise the most suitable mode for long-endurance missions. The comparative evaluation of Eppler E205, Selig S1223, and MH60 airfoils revealed that although S1223 provides high lift and MH60 exhibits moderate performance, the Eppler E205 airfoil offers a superior balance of aerodynamic characteristics. It achieves stable lift generation, comparatively lower drag, and a higher lift-to-drag ratio, along with gradual stall behavior that enhances flight stability and operational safety.

The CFD analysis performed using SU2 confirmed these findings, showing near-linear lift variation within the operational range and peak aerodynamic efficiency under cruise conditions. Validation against OpenVSP results demonstrated strong agreement in aerodynamic trends, thereby confirming the reliability and accuracy of the computational approach, with minor deviations in drag attributed to viscous effects and flow separation captured in CFD simulations.

A significant outcome of this study is the enhancement in UAV performance achieved through aerodynamic optimization. The implementation of the Eppler E205 airfoil combined with constant cruise operation resulted in an approximate 21%

improvement in aerodynamic efficiency, leading to an estimated 25–30% increase in flight endurance under optimal operating conditions. These improvements directly contribute to reduced energy consumption and extended flight duration, which are critical for continuous and large-area wildlife monitoring missions.

Overall, the proposed UAV configuration demonstrates high aerodynamic efficiency, stability, and reliability. The study establishes that the Eppler E205 airfoil operating under constant cruise conditions provides an optimal solution for achieving long-endurance performance in fixed-wing UAV applications.

REFERENCES

[1] Pliakos, C., Efrem, G., Terzis, D. and Panagiotou, P. 2025b. An automated framework for streamlined CFD-based design and optimization of fixed-wing UAV wings. Algorithms, 18(4): 186.

[2] Sahraoui, M., Boutemedjet, A., Mekadem, M. and Scholz, D. 2024b. Automated design process of a fixed wing UAV maximizing endurance. Journal of Applied Fluid Mechanics, 17(11).

[3] Orozco, C., Vásquez, S., Caratt, J., De Armas, N. and Guarín, A. 2025. CFD-based study of aerodynamic performance in UAVs under adverse pressure gradient conditions. Procedia Computer Science, 257: 1213–1220.

[4] İnan, A. T. and Ceylan, M. 2024b. Aerodynamic analysis of fixed-wing unmanned aerial vehicles moving in swarm. Applied Sciences, 14(15): 6463.

[5] Kassa, B. Y., Baheta, A. T. and Beyene, A. 2024b. Aerodynamic performance characteristics of low Re airfoils: A parametric and multi criteria decision study. Results in Engineering, 24: 103174.

[6] Liao, Y., Cheng, K., Sun, W., Zhao, Y., Jia, X. and Qi, W. 2024b. Computational fluid dynamics analysis of aerodynamic characteristics in long-endurance unmanned aerial vehicles. Heliyon, 10(19): e38804.

[7] Sachs, G. 2025. Powered-gliding/climbing flight performed by bats for saving fuel. Biology Open, 14(8).

[8] Kapoulas, I. K., Statharas, J. C. C., Hatziefremidis, A. and Baldoukas, A. K. 2022b. Fast airfoil selection methodology for small unmanned aerial vehicles. Applied Sciences, 12(18): 9328.

[9] Olodu, D. D., Ihenyen, O. I. and Erameh, A. 2025. Numerical and experimental analysis of aerodynamic performance in next-generation unmanned aerial vehicles (UAVs). Journal of Engineering and Basic Sciences, 04: 43–55.

[10] Uzun, M. 2025. Impact of aspect ratio on structural integrity and aerodynamic performance in fixed-wing UAV. Journal of Aviation, 9(1): 19–27.

[11] Abdykadyrov, A., Ibekeyev, S., Analiyeva, A., Izbairova, A., Altayeva, Z., Torekul, A., Taissariyeva, K., Imasheva, G., Abdullaeva, A. and Kystaubayev, N. 2026. Improving the efficiency of fixed-wing unmanned aerial vehicle through the enhancement of aerodynamic and mechanical structures. Applied Sciences, 16(5): 2274.

[12] Morelli, M., Bellosta, T. and Guardone, A. 2021. Development and preliminary assessment of the open-source CFD toolkit SU2 for rotorcraft flows. arXiv preprint arXiv:2107.13895v1.

[13] Fonzi, N., Cavalieri, V., De Gaspari, A. and Ricci, S. 2021. Advances of the Python-based fluid–structure interaction capabilities included in SU2. arXiv preprint arXiv:2109.12332v1.

[14] Colomina, I. and Molina, P. 2014. Unmanned aerial systems for photogrammetry and remote sensing: A review. ISPRS Journal of Photogrammetry and Remote Sensing, 92: 79–97.

[15] Durmuş, S. 2023. Aerodynamic performance comparison of airfoils in flying wing UAV. International Journal of Innovative Engineering Applications, 7(1): 123–127.

[16] Moustafa, M. H., Khashwain, H. S., Dol, S. S. and Ramahi, A. A. 2024b. Enhancing aerodynamic performance in UAV design: CFD analysis. Preprints.org.

[17] Manikandan, M. N. 2025. Aerodynamic optimization of UAVs for increased endurance. International Journal for Research in Applied Science and Engineering Technology, 13(11): 1248–1256.

[18] Chauhan, M. K., Zope, M. and Gorrepati, S. R. 2025. Parametric analysis of wing planforms to determine an optimal wing design. Aviation, 29(1): 11–21.

[19] Linchant, J., Lisein, J., Semeki, J., Lejeune, P. and Vermeulen, C. 2015. Are unmanned aircraft systems (UASs) the future of wildlife monitoring? A review of accomplishments and challenges. Mammal Review, 45(4): 239–252.

[20] Economon, T. D., Palacios, F., Copeland, S. R., Lukaczyk, T. W. and Alonso, J. J. 2015. SU2: an open-source suite for multiphysics simulation and design. AIAA Journal, 54(3): 828–846.

[21] Christie, K. S., Gilbert, S. L., Brown, C. L., Hatfield, M. and Hanson, L. 2016. Unmanned aircraft systems in wildlife research: current and future applications of a transformative technology. Frontiers in Ecology and the Environment, 14(5): 241–251.

[22] Benai-Dara, N. A., Chen, Z. and Kanam, L. K. 2024. Flow control for low-reynolds number airfoil performance enhancement using response surface methodology. International Journal of Science and Research Archive, 13(2): 3019–3029.